This article has been accepted for publication in IEEE Journal of Radio Frequency Identification. This is the author's version which has not been fully edited and content may change prior to final publication. Citation information: DOI 10.1109/JRFID.2026.3680834

Material sensing using arrays of open dipole RAIN RFID tags

Fatima Villa-Gonzalez, *Member, IEEE,* Rahul Bhattacharyya, *Senior Member, IEEE,*
and Pavel Nikitin, *Fellow, IEEE,*

***Abstract*—This work demonstrates how open dipole (OD) RAIN RFID tags and tag-arrays can be used for material characterization in a standard compliant way. Unlike T-matched antennas, OD designs exhibit reduced resonance complexity, with a single minimum in the power-on-tag-forward (POTF) and a single maximum in the power-on-tag-reverse (POTR) response. We introduce a setup-invariant metric based on the transmitted and received reader powers at tag threshold, which preserves resonance information while eliminating the need for calibration. In addition, we demonstrate that auto-tune (AT) code changes in self-tuning ICs of OD tags provide clear and narrowband min-max transitions that remain stable over a wide range of transmit powers, providing high tuning flexibility and enabling sensing at fixed reader power. Building on this, we propose a novel approach for material sensing, leveraging the AT-code transitions within the narrow UHF RFID band using arrays of individually tuned OD tags. We demonstrate the repeatability of open dipole-based sensing using 6 commercial OD RAIN RFID tags to estimate the effective dielectric permittivity of 7 materials, obtaining lower variance than T-matched antennas for high ε_r dielectrics. Furthermore, we propose a custom three OD tag array capable of discriminating between four specific materials and air within the UHF band, demonstrating the sensing capability of this new method in compliance with regulatory standards.**

***Index Terms*—Open dipole antenna, material sensing, RAIN RFID tags, auto-tuning ICs, power-on-tag-forward, power-on-tag-reverse**

I. INTRODUCTION

Radio-frequency identification (RFID) has grown into a large-scale industrial technology, with billions of passive UHF tags deployed annually across retail, logistics, and manufacturing sectors [1]. Continued reductions in tag cost and advances in chip and antenna design are pushing RFID into new sectors such as structural health monitoring [2], biomedical industry or smart agriculture [3], among others. This widespread deployment creates an opportunity to leverage RFID tags as low-cost, ubiquitous sensing elements, rather than only as identifiers [4].

Concurrently, waste management and material recovery systems are undergoing active modernization, driven by regulatory pressure, such as Walmart's mandate for item-level tagging [5], and sustainability targets [6]. Material recovery facilities worldwide increasingly rely on advanced sensing, automation, and data-driven sorting to address contamination and material complexity [7]. However, many of these techniques are slow, and often require line-of-sight, which can limit their throughput and accuracy [8]. Embedding sensing capabilities into RFID tags already present on packaging offers a practical pathway to leverage the inherent wireless benefits of this technology, improving material identification and sorting efficiency without the need for additional sensing hardware.

RAIN RFID tags are commonly characterized by threshold sensitivity and backscatter responses, referred to as threshold power-on-tag-forward (POTF) and threshold power-on-tag-reverse (POTR), respectively [9]. While T-matched antennas formed by a dipole coupled to an inductive loop [10] are well suited for ARC (RFID Assessment and Certification) scenarios involving multiple item types [11] due to their broadband impedance matching, their resonance behavior is inherently complex. As demonstrated by Nikitin *et al.*, POTF resonances of T-matched tags are complicated functions of dipole, loop, coupling and chip impedance characteristics. T-matched tags exhibit three distinct resonant frequencies, f_a, f_b and f_c (see Fig. 1) [12]. Building on this, Nikitin *et al.* also demonstrated that shifts in f_c can be used to extract the effective dielectric permittivity ε_{eff} of tagged materials [13], [14], while shifts in f_a, f_b and f_c enable estimation of effective magnetic permeability μ_{eff} [15].

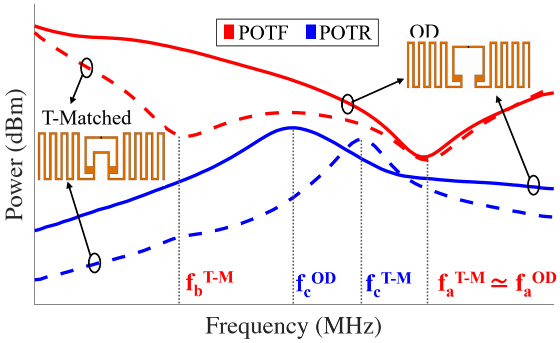

Fig. 1. Representative POTR (blue) and POTF (red) curves of a T-matched (T-M) RAIN RFID tag (dashed) and its open dipole (OD) version (solid) with their resonances marked.

Recently, the same authors derived original closed-form formulas for open dipole (OD) RFID tag resonances [16], showing that the absence of a loop eliminates coupled resonant modes, resulting in simpler POTF and POTR responses with only two resonances f_a and f_c (see Fig. 1). Although the operational frequency bandwidth of ODs is narrower than that of T-match designs, the measured resonance shifts reported in [16] for OD RAIN tags placed on different material types, suggest that their direct relationship to dielectric permittivity and permeability could simplify and make material sensing in the UHF RFID band more practical. Besides, ODs can be made more compact (e.g., miniature tagging) because no inductive matching loop is needed [17], [18].

In practice, RFID measurements are challenged by factors like propagation noise, the geometry of the measurement

Fatima Villa-Gonzalez and Rahul Bhattacharyya are with the Auto ID Labs, Massachusetts Institute of Technology (MIT), Cambridge, MA 02139 (e-mail:rahul_b@mit.edu; fatimavi@mit.edu)

Pavel Nikitin is with Impinj, Seattle, WA 98109 (e-mail: nikitin@ieee.org)

This article has been accepted for publication in IEEE Journal of Radio Frequency Identification. This is the author's version which has not been fully edited and content may change prior to final publication. Citation information: DOI 10.1109/JRFID.2026.3680834

setup, and variations in the surrounding environment [19] [20]. Consequently, acquiring the POTF and POTR curves typically requires careful environmental calibration using a reference tag, along with a precision wideband tag power measurement reader [9]. Calibration based on a reference tag is only valid within a limited spatial region around the reference location; when sensing tags are displaced from this region, POTF and POTR values inferred from such calibration may become inaccurate. Therefore, eliminating the need of calibration is particularly appealing for practical sensing scenarios with moving tags, such as conveyor-belts, or with spatially distributed tags and tag arrays.

To mitigate these limitations and enable more robust extraction of the analog information from the tag, alternative approaches that avoid POTF and/or POTR curve measurement have been proposed. Notably, Nikitin *et al.* derived a setup-independent relationship between the transmitted power and the reader sensitivity by combining the forward and reverse link budgets, showing that the product of these quantities depends only on tag (chip and antenna) parameters and is valid for arbitrary propagation environments as was shown in [21] and discussed later in [22]. Similarly, Marrocco *et al.* introduced the concept of an Analog Identifier (AID) [23]–[26], a setup-invariant metric that also combines forward and reverse link information and depends only on the antenna and chip impedances, rather than on the reader–tag geometry or environment. These metrics have been used for sensing [27]–[29]. However, they have not been used explicitly for tag resonance behavior characterization.

As an alternative metric, our previous work introduced a sensing approach based on the auto-tune (AT) code feature available in some RAIN RFID chips (e.g., recent generations of Impinj ICs [30]) which support adaptive capacitance adjustments for antenna impedance matching [31]. We demonstrated that transitions of the AT code across frequency can be used to estimate the POTF resonance frequencies (f_a and f_b) and dipole resonance frequency (f_1) of antennas with a T-match structure without the need for generating the POTF and POTR curves. Furthermore, we showed that the POTR resonance (f_c) and loop resonance frequency (f_2) can be derived from these markers and used to estimate both ε_{eff} and μ_{eff} of materials. This method did not require to precisely measure reader output or received power, have knowledge of the environment or read distance, nor disable the auto-tune functionality in order to determine the resonance frequencies [32], [33].

Nevertheless, one of the main limitations of using the AT code with T-matched antennas is that their inductive loop introduces coupled resonant modes, resulting in broadband, irregular AT-code transitions that do not always span the full AT range and may lead to ambiguous and distorted resonances, increasing false detections and sensing errors [31]. Additionally, this approach relies on sweeping a wide frequency range (600–1300 MHz) in order to capture all the relevant AT-code transitions of T-matched antennas. Moreover, because the chip input impedance depends on the incident power level, measurements must be performed at tag threshold power, whose determination is time consuming. Together, these constraints limit direct applicability of the AT-based method with standard commercial readers, which typically operate over narrow UHF bands (860-960 MHz), and provide fixed or coarsely adjustable output power [34].

With the goal of making RAIN RFID-based material sensing more accurate, practical and standard compliant, this work proposes using open dipole RAIN RFID tags and tag-arrays for material characterization. The material sensing approaches demonstrated in this paper are summarized in Table I and are as follows:

1) We first validate that the effective dielectric permittivity, ε_{eff}, of materials can be directly estimated from the f_a and f_c resonance shifts detected in POTF and POTR measurements of OD tags.
2) We then propose using a setup-invariant metric for sensing, which we denote as *Power Product (PP)* and is based on the transmitted and received reader powers at tag threshold ($P_{TX} \cdot P_{RX}$). We prove that this metric preserves resonance information and does not depend on the reader-tag configuration, eliminating the need of measuring POTF/POTR curves. The PP also decreases data and processing complexity by enabling identification of multiple resonances from a single curve.
3) We demonstrate that AT-code changes in OD tags with self-tuning ICs exhibit sharp and clear narrowband min-max transitions at f_a and f_1, providing high tuning flexibility through dipole length trimming and finer resonance detection precision than T-matched tags. Additionally, we further prove that, AT-code changes remain stable over a wide range of transmit powers, enabling calibration-free sensing at fixed reader power.
4) Finally, we propose a novel approach for material sensing within the narrow FCC UHF RFID band (902–928 MHz) by leveraging the consistent narrowband AT-code transitions of OD tags, which we intentionally tune to respond to different materials.

The rest of the paper is organized as follows. Section II validates the use of open-dipole RAIN RFID tags for material sensing using three complementary methodologies. Section III introduces the proposed custom-designed array approach for narrowband sensing. Section IV describes the tags used, materials tested, hardware setup and the data capture procedure. Sections V and VI present material sensing results using individual open dipoles and custom-designed OD tag arrays, respectively. Finally, Section VII presents the main conclusions and future research directions.

II. MATERIAL SENSING WITH OPEN DIPOLE RAIN TAGS

A. Material sensing from POTF and POTR curves

As discussed in the introduction, RFID tags employing open dipole antennas exhibit a simpler resonance behavior than tags based on T-matched antenna structures. T-matched tags have three characteristic resonant frequencies f_a, f_b and f_c that originate from the interaction between the natural resonant frequency of the dipole (f_1) and that of the inductive loop (f_2), as captured by the closed-form circuit expressions for the characteristic angular frequencies ($\omega = 2\pi f$) derived in Eq. (4) and (8) in [12] and summarized in Table II.

This article has been accepted for publication in IEEE Journal of Radio Frequency Identification. This is the author's version which has not been fully edited and content may change prior to final publication. Citation information: DOI 10.1109/JRFID.2026.3680834

TABLE I
MATERIAL SENSING APPROACHES DEMONSTRATED IN THIS PAPER USING OD RAIN TAGS WITH/WITHOUT AUTO-TUNING ICS.

Monitored parameters	**How are they monitored?**	**Number of tags**	**Require calibration with known tag?**	**Require reading AT?**	**Require disabling AT?**	**Measurable at fixed transmit power?**	**What chips can be used?**	**Examples of specific chips**
Tag resonances	Threshold POTF and POTR curves	Single or multiple (wideband equipment needed)	No, if only the resonance frequencies are needed	No	Yes	No	Any (with or without AT, as long as AT can be disabled)	**Without AT:** any **With AT:** Monza R6, M700, M800, U8, U9[1]
	Threshold P_{TX} and P_{RX} curves (*Power Product*)		No	No	Yes	No		
	AT code transitions	Single or multiple (wideband equipment needed)	No	Yes	No	Yes	Chips with AT where AT code is readable	**With AT:** Monza R6, M700, M800, Magnus[2]
		Multiple individually tuned tags (can use narrowband reader)						

[1] NXP U8, U9 ICs have AT feature (i.e., self-adjust) but AT state is not readable.
[2] AT of Magnus IC cannot be disabled (but AT code can be read).

In contrast, OD tags do not include an inductive matching loop and therefore do not exhibit a loop-related resonance. As a result, they are characterized by only two resonances, f_a and f_c. As shown by the analytical expressions derived in Eq. (1) and (4) [16] and reported in Table II, for most RFID tags, f_c coincides exactly with f_1 (see Appendix A).

TABLE II
COMPARISON OF CHARACTERISTIC ANGULAR FREQUENCIES OF RFID TAGS WITH T-MATCHED AND OD ANTENNA STRUCTURES

ω	**Definition**	**Formula**	
		T-matched	**OD**
ω_1	Natural res. freq. of dipole	$\omega_1 = \frac{1}{\sqrt{L_1 C_1}}$	
ω_2	Natural res. freq. of loop	$\omega_2 = \frac{1}{\sqrt{L_2 C_p}}$	–
ω_a	Lower POTF res. freq.	$\omega_{a,b}^2 = \frac{\omega_1^2+\omega_2^2}{2(1-k^2)} \pm$ $\pm \frac{\sqrt{(\omega_1^2-\omega_2^2)+4k^2\omega_1^2\omega_2^2}}{2(1-k^2)}$	$\omega_a = \omega_1\sqrt{1+\frac{C_1}{C_p}}$
ω_b	Higher POTF res. freq.		–
ω_c	POTR res. freq.	$\omega_c^2 = \frac{\omega_1^2}{1-k^2}$	$\omega_c = \omega_1$
k	Coupling coefficient	$k = \sqrt{1-\frac{\omega_2^2}{\omega_a^2+\omega_b^2-\omega_c^2}}$	–

To illustrate these differences, we performed full-wave electromagnetic simulations in HFSS of the commercial Beontag A701 T-matched RFID tag [35], as well as a modified version of the same antenna in which the inductive loop trace was removed to realize an OD configuration in air (see overlays in Fig. 1). Based on the antenna impedances obtained in the simulations, the corresponding POTF and POTR responses were computed in Matlab using the analytical expressions in [12], specifically Eq. (2) for POTF and Eq. (5) for POTR.

Fig. 2 shows the resulting POTF and POTR curves for both antenna configurations when loaded with an Impinj Monza M700 series IC, assuming a base load capacitance (chip + mount) of $C_{p'} = 1.04$ pF and a chip sensitivity of -21.85 dBm (-24 dBm plus the gain of an ideal dipole antenna (2.15 dBi) [36]). In the calculations, the antenna gain was assumed constant across the band ($G = -0.75$ dBi), the polarization mismatch factor was set to $p = 1$, and the modulation resistance was assumed to be $R_{mod} = 30\ \Omega$.

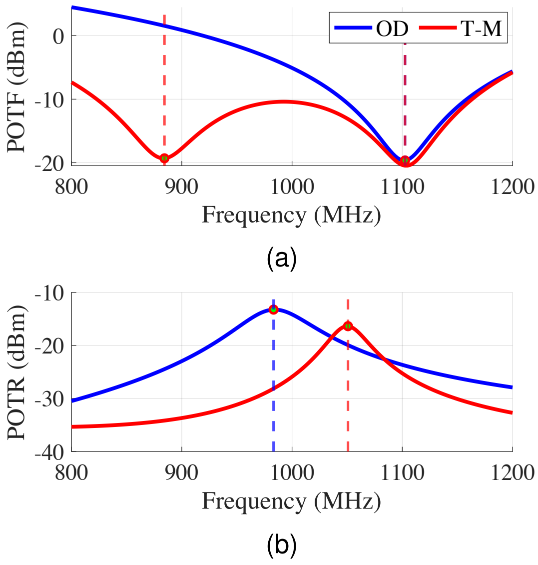

(a)

(b)

Fig. 2. Computed (a) POTF and (b) POTR curves of the Beontag A701 RAIN RFID tag with a T-matched (T-M) antenna (orange) and its open dipole (OD) version (blue), with the resonances detected from the POTF/POTR curves marked with dashed lines.

As expected, for the T-matched antenna, the POTF response exhibits two minima corresponding to f_a and f_b. When the inductive loop is removed in ODs, the lower-frequency POTF resonance associated with the loop, f_b, disappears, leaving only the upper POTF resonance f_a, which is associated with the dipole mode and remains at a similar frequency. In addition, the maximum of the POTR response for the OD shifts with respect to the T-matched case and coincides with the natural resonance of the dipole, ($f_c = f_1$), in agreement with the analytical expressions for OD tags in Table II. As expected, the POTF resonance of the RFID tag with OD antenna is higher than its POTR resonance [16] (see Appendix A).

Because the dipole natural resonance f_1 is determined by the equivalent series inductance L_1 and capacitance C_1 of the dipole around its main resonance, and since C_1 is strongly influenced by the surrounding material, this direct correspondence enables a simplified estimation of ε_{eff} from the measured POTR resonance. In particular, for dielectric

This article has been accepted for publication in IEEE Journal of Radio Frequency Identification. This is the author's version which has not been fully edited and content may change prior to final publication. Citation information: DOI 10.1109/JRFID.2026.3680834

materials ($\mu_r \approx 1$), ε_{eff} can be estimated directly from the shift of f_c on a Material Under Test (MUT), f_c^{MUT}, relative to its value in air, f_c^{air}, as

$$\varepsilon_{eff} = \frac{1}{(1-\Delta_1)^2}, \text{ where } \Delta_1 = \frac{f_c^{air} - f_c^{MUT}}{f_c^{air}}, \tag{1}$$

which can be simplified as

$$\varepsilon_{eff} = \left(\frac{f_c^{air}}{f_c^{MUT}}\right)^2. \tag{2}$$

Alternatively, simultaneous detection of the resonance frequencies f_a and f_1 from the POTF and POTR responses of an OD tag enables direct extraction of L_1 and C_1 which can then be used to estimate both ε_{eff} and μ_{eff} [15]. From the expression of ω_a in Table II for ODs, we obtain:

$$C_1 = C_p\left(\frac{\omega_a^2}{\omega_1^2} - 1\right), \tag{3}$$

which allows C_1 to be determined when the chip capacitance C_p is known. Once C_1 is known from above, L_1 follows directly from ω_1:

$$L_1 = 1/\omega_1^2 C_1. \tag{4}$$

B. Power Product for material sensing from P_{TX} and P_{RX} curves

In addition to extracting material information from POTF and POTR curves individually, further simplification can be achieved by considering their product, here referred to as the Power Product (PP)

$$\mathrm{PP} = \mathrm{POTF} \cdot \mathrm{POTR} \tag{5}$$

$$\mathrm{PP_{dB}} = \mathrm{POTF_{dB}} + \mathrm{POTR_{dB}} \tag{6}$$

in linear scale and logarithmic scale, respectively. The PP combines threshold sensitivity and backscatter responses into a single curve while preserving all antenna resonance features, thereby reducing the amount of data to be processed and simplifying resonance identification.

Beyond processing simplicity, a key advantage of the PP is that it can be obtained directly from reader-side measurements without the need of computing POTF and POTR. As shown in Appendix B, the product of the transmit and received powers at the reader when the tag is operating at threshold, P_{TX} and P_{RX}, respectively, satisfies

$$P_{\mathrm{TX}} \cdot P_{\mathrm{RX}} = \mathrm{POTF} \cdot \mathrm{POTR}. \tag{7}$$

Importantly, P_{TX} and P_{RX} are quantities directly available at the reader, whereas explicit determination of POTF and POTR typically requires knowledge of the reader–tag distance and propagation environment. The latter is further proven in Appendix C, resulting in

$$\mathrm{POTF} \cdot \mathrm{POTR} = P_{\mathrm{ic}}^2 \cdot \frac{|Z_c + Z_a|^2}{16 R_c^2} \cdot \frac{|Z_c|^2}{|Z_a|^2}, \tag{8}$$

which depends only on the antenna and chip impedances, $Z_a = R_a + jX_a$ and $Z_c = R_c + jX_c$, and IC sensitivity P_{ic}, and thus can be considered setup independent.

Furthermore, it can be seen that the power product preserves all characteristic resonance frequencies of the tag. The extrema of (8) are determined solely by the ratio $|Z_c + Z_a|/|Z_a|$. POTF is minimized when the antenna and chip impedances are closest to complex conjugate matching, i.e., when $|Z_c + Z_a|$ is minimized. Consequently, minima of $|Z_c + Z_a|$ directly correspond to minima of the POTF curve. Similarly, POTR reaches a maximum when $|Z_a|$ is minimized, which occurs at the antenna's natural resonance where the reactance vanishes ($X_a = 0$). Hence, the minima of $|Z_a|$ correspond to maxima of the POTR response [12]. As a result, we hypothesize that the PP allows resonance extraction and subsequent material parameter estimation without POTF and POTR measurements, thus without calibration.

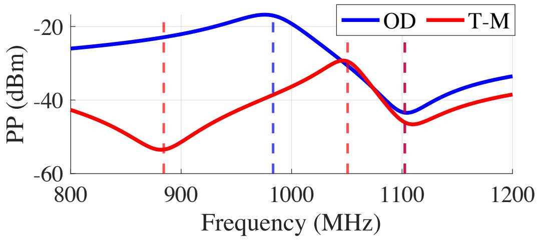

Fig. 3. Computed PP= $\mathrm{POTF}_{dB} + \mathrm{POTR}_{dB}$ for the POTF and POTR curves in Fig. 2 for T-matched (T-M) and OD tags. The relative extrema of the PP coincide with the resonances detected from POTF/POTR (marked with dashed lines).

Fig. 3 presents the PP curves for both the T-matched and OD tags discussed in Section II-A. For T-matched antennas, the PP exhibits three relative extrema, close to f_a, f_b and f_c frequencies. In contrast, for OD tags only two extrema are observed, associated with f_a and f_c. In both cases, the resonance frequencies can be identified directly as stationary points of the PP response, i.e., as zeros of its frequency derivative. Once the PP extrema are identified, the resonance frequency f_c can be extracted and used to estimate ε_{eff} of the MUT using the frequency-shift relationship in (2).

C. Material sensing from AT-code transitions

While AT-code transitions have previously been used to extract resonance frequencies in T-matched RFID tags, in practice, the approach often produced broad, irregular transitions that failed to span the full AT range, leading to ambiguous resonance identification [31]. We demonstrate that this principle is more robustly and simply applied to open dipole tags.

Fig. 4(a) shows the simulated POTF and POTR responses of the OD tag introduced in Section II-A. As discussed earlier, these curves exhibit a single POTF minimum at ω_a and a single POTR maximum at $\omega_c = \omega_1$. Fig. 4(b) presents the corresponding antenna input impedance, Z_a, where R_a and X_a denote the antenna series resistance and reactance, respectively. As expected, the series reactance crosses zero ($X_a = 0$) at the dipole resonance ω_1.

In AT-enabled RFID chips, impedance matching is achieved by adjusting the chip's effective parallel capacitance in order to approach a complex-conjugate match with the antenna

This article has been accepted for publication in IEEE Journal of Radio Frequency Identification. This is the author's version which has not been fully edited and content may change prior to final publication. Citation information: DOI 10.1109/JRFID.2026.3680834

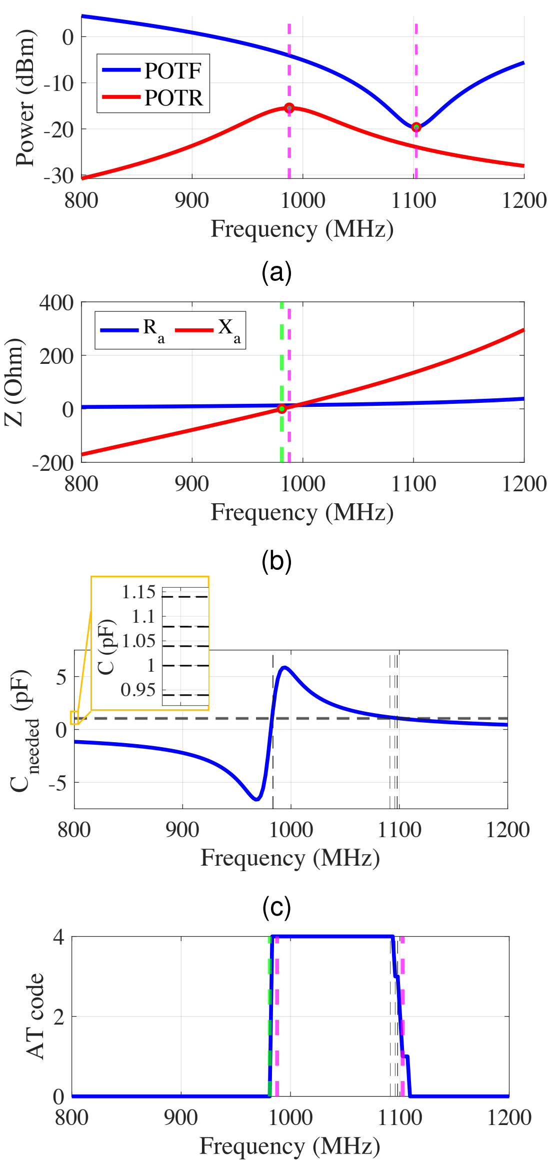

(d)

Fig. 4. Beontag A701 with an OD antenna: (a) POTF and POTR curves with detected resonance frequencies in magenta, (b) Z_a with dipole resonance $X_a = 0$ in green, (c) M750 IC capacitance needed, with discrete C adjustments and crossing points in black, (d) AT code with resonances from POTF/POTR in magenta, $X_a = 0$ in green and C adjustment levels in black.

[37], [38]. As deduced in Appendix D, what determines the matching condition is the antenna parallel reactance, X_{pa}, which depends on both the series resistance and reactance of the antenna. Then, the capacitance required to conjugately match the antenna reactance can be expressed as:

$$C_{\text{needed}} = \frac{1}{\omega X_{pa}} = \frac{X_a}{\omega\left(R_a^2 + X_a^2\right)}. \tag{9}$$

Fig. 4(c) shows the frequency dependence of C_{needed} in (9) together with the discrete capacitance values available through the AT code of the Impinj Monza M700 IC. The chip provides a base parallel capacitance $C_{p'} = 1.04$ pF and five discrete adjustment states corresponding to capacitance offsets of ±40 fF and ±100 fF, encoded by AT codes from 0 to 4.

Fig. 4(d) shows the resulting AT code as a function of frequency. When the required matching capacitance falls outside the available tuning range, the chip saturates at the minimum or maximum AT code (AT = 0 or AT = 4). When C_{needed} lies within the adjustment range, the chip selects the AT code that provides the closest impedance match. Two distinct AT-code transitions are clearly observed in Fig. 4(d): a negative transition whose midpoint is around f_a, and a positive transition at f_1. In fact, the positive AT transition coincides with the frequency at which $X_a = 0$ in Fig. 4(b) (see green vertical dashed line), which is the dipole resonance frequency. We can also notice that this positive AT transition occurs around the resonance detected in the POTR curve (see magenta vertical dashed line, at a slightly higher frequency than the green line). Therefore, these transitions can be used as estimations of the two resonance frequencies of the antenna and, since $\omega_1 = \omega_c$ for ODs, all resonance frequencies relevant to material sensing (Table II) can be extracted directly from the AT-code response.

The frequency-shift relations introduced in Section II-A can now be used to estimate both ε_{eff} and μ_{eff}. Importantly, this AT-code method avoids the need for POTF/POTR curve generation or more complex analytical derivations required for T-matched antennas (see Eq. (1)-(2) in [31]). Besides, in contrast to broadband T-matched antennas, which often exhibit gradual AT-code transitions that do not consistently span the full min–max range and may lead to distorted responses and ambiguous resonance detection [31], OD antennas, due to their narrowband resonance behavior, produce clear and sharp AT-code transitions between minimum and maximum states, enabling not only more reliable and precise resonance identification, but also finer resonance frequency tuning.

However, this method still requires a wideband reader. In the next section, we investigate whether practical AT-code transition-based sensing using OD tags can be used with commercial RFID readers working in the UHF band.

III. NARROWBAND MATERIAL SENSING WITH OPEN DIPOLE RAIN TAG ARRAYS

A. *Concept of material sensing with OD tag arrays*

As a step forward to enable material sensing using standard narrowband commercial RFID readers, we leverage the tuning simplicity of OD RAIN RFID tags, characterized by their distinct, narrowband AT-code transitions. We propose designing arrays of OD tags with intentionally tailored resonance frequencies. By customizing dipole lengths, the free-space resonances of the tags in the array can be distributed such that, for a given dielectric material, at least one tag in the array exhibits a resonance (i.e. an AT-code transition) within the UHF band.

A conceptual diagram of the proposed approach is illustrated in Fig. 5, featuring an array of three OD tags. As shown, when the array is placed on MUT 1, only Tag 1 (optimized for that dielectric) exhibits an AT-code transition within the UHF band. Similarly, Tag 2 provides the transition for MUT 2, and so forth. Since each digital ID (e.g., EPC) is pre-mapped to a specific material profile, the MUT is identified simply by

This article has been accepted for publication in IEEE Journal of Radio Frequency Identification. This is the author's version which has not been fully edited and content may change prior to final publication. Citation information: DOI 10.1109/JRFID.2026.3680834

detecting which tag ID triggers a transition during narrowband measurement. Besides, since the AT code method is used, no calibration with a reference tag is required and the reader can transmit a fixed power.

B. Resonance frequency tuning for RAIN OD tag array design

Let $f_i^{\mathrm{MUT}i}$ denote one resonance frequency (either f_a or f_1) of a given tag i when the tag is attached to a given MUT i. The array design condition is that, at least for one tag in the array,

$$f_i^{\mathrm{MUT}i} \in [f_{\min}, f_{\max}], \tag{10}$$

where $[f_{\min}, f_{\max}] = [902, 928]$ MHz is the UHF RFID band.

Because most standard RAIN RFID tags exhibit a resonant frequency $f_i^{\mathrm{MUT}i}$ lower than the minimum UHF operating frequency (f_{min}) when loaded with a MUT, the condition in (10) can be met by progressively shortening the dipole. This reduction in length increases $f_i^{\mathrm{MUT}i}$ until the resonance shifts into the detectable UHF band. Analytically, this tuning procedure is expressed as:

$$f_i^{\mathrm{MUT}i} + \Delta f_{Li}^{MUTi} \approx f_{mid}^{UHF}, \tag{11}$$

where $f_{mid}^{\mathrm{UHF}} = 915$ MHz represents the center of the UHF band, and $\Delta f_{Li}^{\mathrm{MUT}i}$ is the positive frequency shift resulting from the reduction in physical dipole length, L_i, required to detect $MUTi$.

To ensure continuous sensing coverage across a wide range of material properties, each dipole lengths L_i is calculated to compensate for a specific dielectric load, effectively 'pre-tuning' each tag so that its resonance enters the UHF band only when a material within a target permittivity range is present. While L_i is typically optimized to shift the positive transition, f_1, into the UHF band, a tag can be further tailored to utilize the negative transition marker f_a. This flexibility allows a single tag to potentially identify multiple materials: for instance, exhibiting a positive transition for a lower-permittivity MUT and a negative transition for a higher-permittivity MUT.

Furthermore, the physical separation between adjacent OD tags in the array is optimized to minimize mutual coupling, ensuring that the AT-code transition of the active tag remains sharp and independent of the surrounding array elements.

IV. EXPERIMENTAL SETUP

This section describes the RAIN RFID tags and materials used, the reader hardware, the measurement environment, and the data acquisition procedure.

A. RAIN RFID tags

The Beontag A701 RAIN RFID tag was used as the primary platform to experimentally validate the proposed material sensing approaches described in Sections II for the single-tag configuration and in Section III for the tag-array implementation. This tag was selected due to its well-characterized impedance behavior, availability of an AT-enabled Impinj Monza M750 chip and stable performance across different material loadings. Although the original A701 tag employs a T-matched antenna structure, the inductive loop was removed (i.e., cut), as illustrated in Fig. 6, to convert the antenna into an open dipole configuration consistent with the proposed sensing framework.

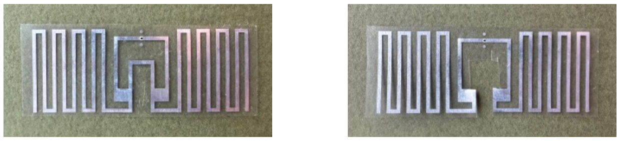
(a) (b)

Fig. 6. (a) Original Beontag A701 with a T-matched antenna and (b) modified open dipole version with the loop cut.

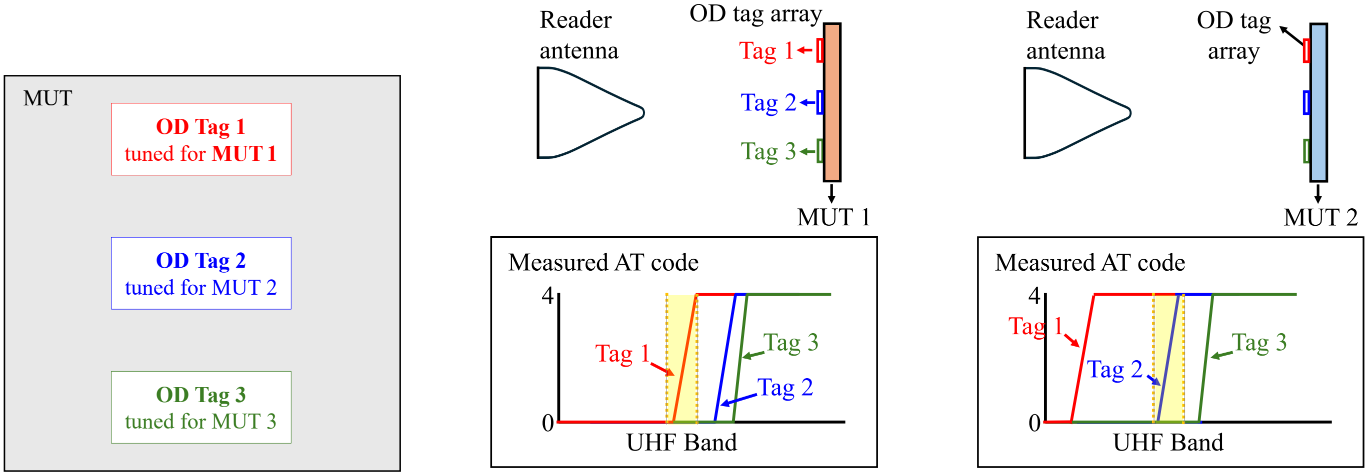

(a) (b) (c)

Fig. 5. Conceptual diagram of the proposed narrowband material sensing approach using OD RAIN tag arrays: (a) An array of three OD tags, where each tag is optimized to shift f_1 into the UHF band upon contact with a specific target material. (b) Illustrative response when the array is attached to MUT 1; only the EPC associated with Tag 1 exhibits an AT-code transition within the operational bandwidth, enabling material identification. (c) Response when the array is attached to MUT 2; in this case, MUT 2 shifts the resonance of Tag 2 into the UHF band, while Tag 1 and Tag 3 remain out-of-band. The resulting transition in Tag 2's AT code provides a unique identifier for MUT 2.

This article has been accepted for publication in IEEE Journal of Radio Frequency Identification. This is the author's version which has not been fully edited and content may change prior to final publication. Citation information: DOI 10.1109/JRFID.2026.3680834

In addition to the A701 tag, several other commercial RAIN RFID tags were tested to provide broader experimental validation of material sensing with OD tags. These tags, included in Table III, feature different antenna geometries and incorporate three distinct RFID chips with auto-tuning capabilities (AT codes 0 through 4 and parallel capacitance adjustments of up to ± 100 fF). All tags originally employed T-matched antenna designs [39] and were similarly modified by removing the inductive loop to form OD antennas.

TABLE III
OD RAIN RFID TAGS USED IN THIS STUDY

Model	**Size (mm)**	**IC**	**R_p (Ohm)**	**$C_{p'}$[1] (pF)**	**Image**
Beontag A701	42 x 16	Impinj Monza M750	2800	1.04	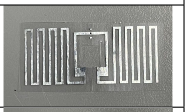
Arizon AZ-MR71	42 x 16	Impinj Monza M730	2800	1.04	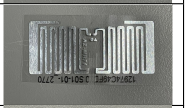
Beontag E702	70 x 14				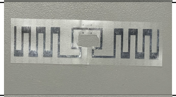
Arizon AZ-HR7G	71.5x 18				
Arizon AR-61F	40 x 15	Impinj Monza R6	1200	1.44	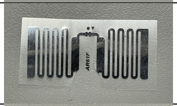
Beontag H61	50 x 30				

[1] Total load capacitance: $C_{p'} = C_p + C_{mount}$, where C_p is the intrinsic capacitance of the IC and C_{mount} is the mounting capacitance.

B. Materials tested

We use the Voyantic material kit in in Fig. 7 for ϵ_{eff} estimation [40]. Their size is 130 x 130 mm, thickness is 4 mm and their dielectric properties are summarized in Table IV.

Fig. 7. Materials in the Voyantic kit used for sensing.

TABLE IV
MATERIAL PROPERTIES IN THE VOYANTIC KIT

Material	**ϵ_r**	**$tan(\delta)$**
PTFE	2.05	0.0002
Cardboard (CB)	2.57	0.0717
POM	2.96	0.0450
PVC	3.00	0.0079
FR4	4.87	0.0141
Rubber	6.73	0.0247
Glass	7.11	0.0098

C. Reader hardware and test setup

The experimental setup for material sensing is illustrated in Fig. 8. For RFID tag characterization and demonstration purposes, we employ the Voyantic Tagformance Broadband kit [9] to take measurements over the 600–1300 MHz frequency range. The RFID tags are attached to the MUTs using adhesive tape and mounted vertically at a distance of 30 cm from the horizontally positioned reader antenna. A foam spacer is used to ensure consistent separation and to maintain the tags flat against the surfaces of the MUTs. Foam absorbers are placed behind the tag to mitigate environmental reflections around the setup. The behavior of the resonances will remain consistent regardless of polarization alignment between the reader antenna and the tags [31].

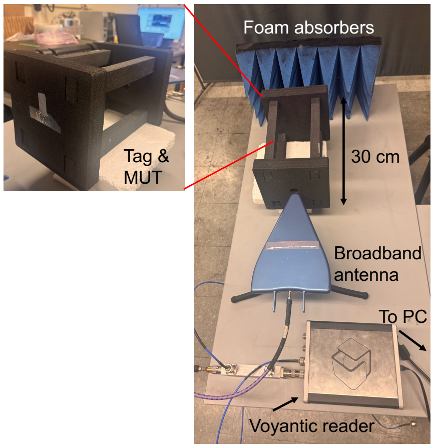

Fig. 8. Experimental setup.

D. Data capture procedure

The measurement procedure consists of the following steps:

- First, a threshold power sweep is performed with the AT feature enabled. During this sweep, the POTR response and the corresponding AT-code variation are recorded over the 600–1300 MHz frequency range.
- Second, the AT feature is disabled and the threshold sweep is repeated to extract the POTF curve. This step is required because, as indicated in Table II, ω_a depends on the chip impedance, which can be modified when AT is active. The transmitted and received powers at the reader, P_{TX} and P_{RX}, are recorded.

Experiments are conducted using the *Read 640K FM0* mode of the Voyantic system, which corresponds to the highest read-rate mode supported by the EPC Gen2 protocol. This mode enables rapid access to the tag memory, thereby improving the efficiency and throughput of the measurement process.

V. RESULTS OF MATERIAL SENSING USING AN OD TAG

A. Validation of resonance monitoring methods

Fig. 9 experimentally demonstrates the validity of the resonance monitoring methods in Section II using the A701 OD tag shown in Fig. 6(b), evaluated in air, on PVC, and on glass just to give some examples. Fig. 9(a) and (b) show the measured POTF and POTR curves, where the detected resonance frequencies (i.e., POTF minima, f_a and POTR maxima, f_c) for each material are marked with vertical lines.

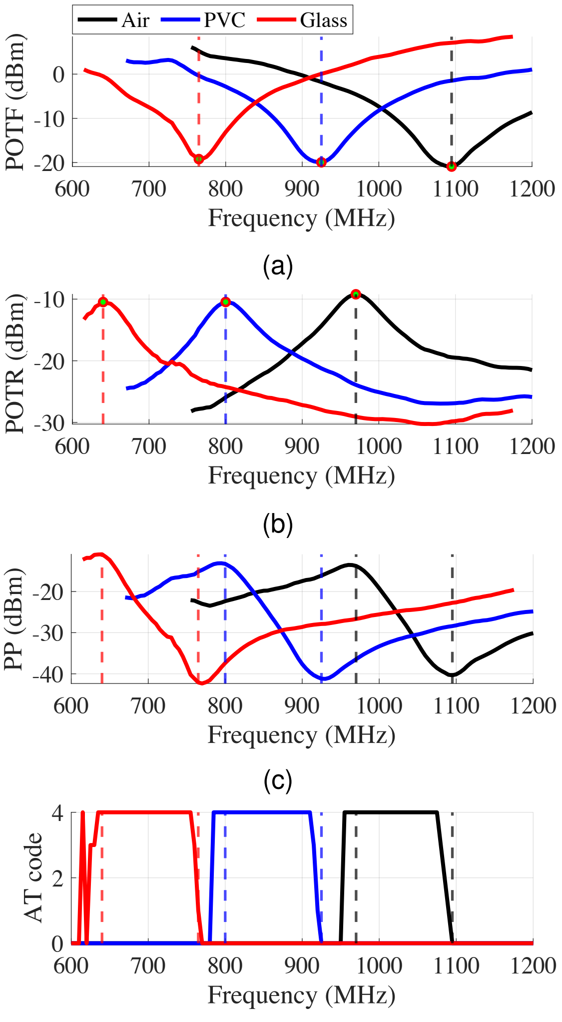

(a)

(b)

(c)

(d)

Fig. 9. Measured (a) POTF, (b) POTR, (c) $\text{PP} = \text{POTF} \cdot \text{POTR}$ and (d) AT code state for the OD Beontag A701 RAIN RFID tag. The resonance frequencies detected from POTF/POTR are marked with dashed vertical lines and coincide with the PP extrema and are close to AT-code transitions.

Fig. 9(c) shows the computed Power Product (PP) curve from both expressions in (7) (i.e, $\text{POTF} \cdot \text{POTR} = P_{TX} \cdot P_{RX}$). Both products in (7) yield equivalent curves with relative extrema around the POTF minima and and POTR maxima from Fig. 9(a) and (b) (see vertical dashed lines). Fig. 9(d) shows the measured AT codes across frequency. The vertical dashed lines correspond to f_a and f_c, detected from POTF/POTR curves. The f_a marker aligns with the midpoint of the negative AT slope. For all MUTs, the f_c marker shows a small offset towards higher frequencies with respect to the positive AT transition. This aligns with the simulations in Fig. 4, where the offset is driven by R_{mod} (see Appendix A).

Table V quantifies the values of f_a and $f_c = f_1$ detected using the three methods in Section II (summarized in Table I): (1) directly from POTF/POTR curves, (2) from the derivatives of the PP curves, and (3) from AT-code transitions, for all the dielectric materials in Section IV-C using the Beontag A701 OD. We use these detected frequencies to compute the estimated values of equivalent L_1 and C_1 using (3) and (4), respectively. Finally, we estimate the ε_{eff} of the materials with all the obtained variables applying (2) and compare the accuracy of the results obtained with each method.

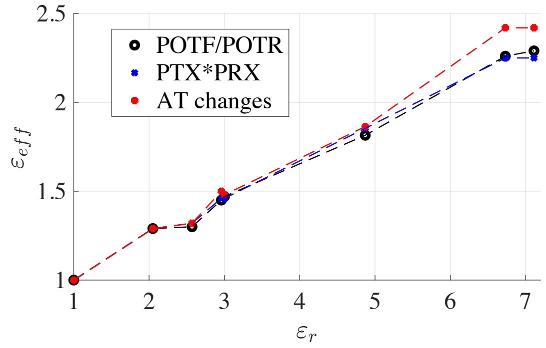

Fig. 10. Relationship between estimated ϵ_{eff} and MUT ϵ_r for the Beontag A701 OD using the three proposed methods.

Fig. 10 shows the relationship between the estimated ε_{eff} values and the relative permittivity ε_r of the dielectric materials for the Beontag A701 OD. The expected linear relationship is observed for all the methods. The AT-code based monitoring gives slightly higher ε_{eff} values, especially for higher ε_r.

To demonstrate that material sensing with ODs is applicable across a range of commercial RAIN tags, ε_{eff} has been estimated for the six OD tags in Table III using their POTF and POTR measurements. Fig. 11 shows the mean and standard deviation of the ε_{eff} values estimated as a function of the relative permittivity ε_r of the dielectric materials. The relationship is linear and consistent for both tested methods. The estimated ε_{eff} show slightly larger standard errors for higher values of ε_r. This can be attributed to increased sensitivity to small air gaps between the tag and high ε_r material surface, which may result from slight sagging of flexible samples or minor imperfections in tag attachment.

Overall, these effects and trends are in agreement with expected ε_{eff} values [41], with open dipole tags showing lower variance (0.16) than the T-matched configuration (0.18) [13]. Thus, they support the conclusion that open dipole tags can be used effectively and reliably for dielectric sensing. From a practical standpoint, resonance detection with ODs is less ambiguous than with T-matched antennas and avoids

This article has been accepted for publication in IEEE Journal of Radio Frequency Identification. This is the author's version which has not been fully edited and content may change prior to final publication. Citation information: DOI 10.1109/JRFID.2026.3680834

TABLE V

DETECTED VALUES OF f_a AND $f_1 = f_c$, COMPUTED C_1 AND L_1 VALUES USING (3) AND (4), WITH BASE $C_{p'}$ =1.04 pF (AUTOTUNE TURNED OFF), AND ESTIMATED ε_{eff} FOR THE A701 OD TAG ON DIFFERENT MUTS USING THE THREE PROPOSED RESONANCE MONITORING METHODS.

Resonance monitoring method	**Parameter**	**Materials**							
		Air	**PTFE**	**CB**	**POM**	**PVC**	**FR4**	**RUBBER**	**GLASS**
Threshold POTF and POTR curves	f_1**(MHz)**	970	855	850	805	800	720	645	640
	f_a**(MHz)**	1095	980	975	930	925	835	775	765
	L_1**(nH)**	3.72	4.19	4.21	4.43	4.46	5.37	5.21	5.47
	C_1**(fF)**	285	326	328	348	350	358	461	446
	ε_{eff}	1	1.29	1.30	1.45	1.47	1.81	2.26	2.29
Threshold P_{TX} and P_{TX} curves (PP)	f_1**(MHz)**	960	845	835	795	795	705	640	640
	f_a**(MHz)**	1095	980	985	940	930	830	780	770
	L_1**(nH)**	3.46	3.90	3.52	3.82	4.12	5.01	4.84	5.24
	C_1**(fF)**	313	359	407	414	383	401	505	465
	ε_{eff}	1	1.29	1.32	1.46	1.46	1.85	2.25	2.25
AT-code transitions	f_1**(MHz)**	953	838	829	778	782	698	613	612
	f_a**(MHz)**	1085	975	963	920	917	840	770	762
	L_1**(nH)**	3.57	3.87	4.00	3.99	4.19	4.40	4.43	4.66
	C_1**(fF)**	308	368	363	414	390	466	601	572
	ε_{eff}	1	1.29	1.32	1.50	1.48	1.86	2.42	2.42

their associated limitations [31]. The narrowband nature of OD resonances, together with the absence of coupled resonant modes, prevents distorted AT-code change trends, resulting in clearer and less ambiguous resonance markers and offering high flexibility for individual tag fine-tuning.

B. Dependence of the AT-code on transmit power

Finally, we demonstrate here an additional practical advantage of the AT-code–based sensing approach by examining the dependence of the AT-code on transmit power. Fig. 12 shows the AT state of a Beontag A701 RFID OD tag in air as a function of frequency and reader transmit power P_{TX}, visualized as a colored surface. AT = 4 is shown in yellow, AT = 0 in dark blue, and white regions correspond to frequencies and power levels below the IC activation threshold, where the tag does not respond. From these plots, it is evident that below a certain transmit power level, P_{AT} (marked by a dashed line), the AT-code transitions remain unchanged and follow the same frequency-dependent trends observed at threshold. At higher transmit power levels, the AT-code transitions begin to change. This behavior indicates that resonance extraction can be performed at a fixed transmit power below P_{AT}, but not necessarily at threshold, further simplifying practical deployment and enabling fast sensing measurements using standard reader power settings.

VI. IMPLEMENTATION OF AN OD TAG ARRAY FOR MATERIAL SENSING

This section details the practical implementation of an OD tag array designed for material sensing within he UHF band. We first examine the resonance tuning of a single OD tag in air and demonstrate the specific design adjustments required to shift the tag's resonance into the UHF band when loaded with a low-permittivity dielectric, such as PTFE. Finally, we describe the integration of these individually tuned elements into a multi-tag array, providing a robust solution for material identification through narrowband AT-code monitoring.

A. Resonance characterization of OD tags in air

From a practical design perspective, the tuning procedure described in Section III-B is implemented by progressively trimming the meandered dipole sections of a commercial RAIN RFID tag.

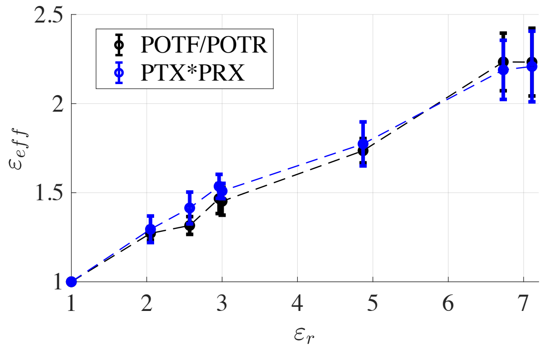

Fig. 11. Relationship between estimated ϵ_{eff} and MUT ϵ_r for six OD versions of RAIN tags.

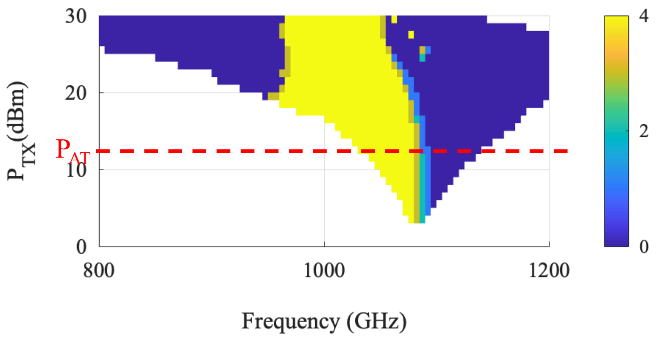

(a)

Fig. 12. Wideband AT code measurements of the Beontag A701 RAIN RFID tag with an OD antenna for different P_{TX} power levels. The color scale corresponds to the AT code values and the power under which the AT code does not change across frequencies is marked with a dashed line.

Fig. 13 illustrates this process using a Beontag A701 OD tag in free-space. The dipole length was reduced in incremental stages: one long segment (-2.1 cm), two long segments (-4.2 cm), a combination of two long and two short segments (-4.6 cm), three long and two short segments (-6.5 cm), and finally four long and three short segments (-9 cm).

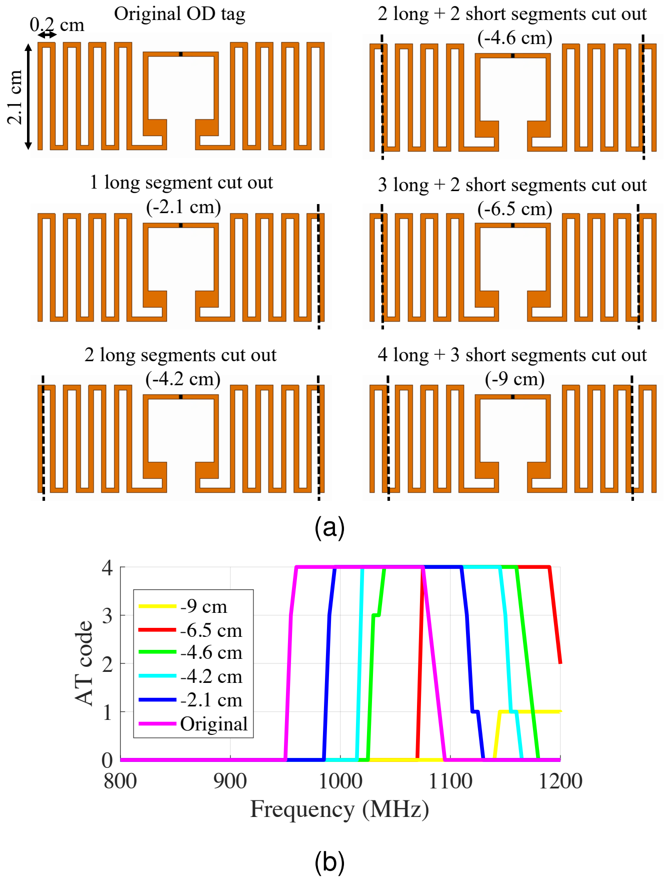

Fig. 13. Tuning process of Beontag A701 OD tag: (a) trimmed progressively 2.1, 4.2, 4.6, 6.5 and 9 cm by cutting the dipoles at the dashed lines, (b) AT-code responses in air shift to higher frequencies as the dipole length decreases.

As quantified in Table VI, both the positive AT-transition frequency (f_1) and the negative transition frequency (f_a) shift upward as the physical length decreases. While this trimming detunes the tag in air, it effectively compensates for the dielectric loading of dielectric materials, shifting the resonance back into the UHF band upon deployment.

TABLE VI
DETECTED SHIFTS OF f_a AND f_1 OF THE TAG IN AIR AS THE DIPOLE LENGTH DECREASES.

	Threshold POTF and POTR curves		**AT-code transitions**	
Dipole trim	Δf_1^{air} **(MHz)**	Δf_a^{air} **(MHz)**	Δf_1^{air} **(MHz)**	Δf_a^{air} **(MHz)**
Original	0	0	0	0
2.1 cm	35	35	36	33
4.2 cm	70	65	64	67
4.6 cm	80	80	75	85
6.5 cm	115	115	119	115
9 cm	205	180	141	190

B. Dielectric loading and tuning: case study on PTFE

As a representative case, we demonstrate the tuning of a single OD tag for PTFE detection. Fig. 14 compares the POTF, POTR, and AT-code responses of an untrimmed Beontag A701 tag in free-space and on PTFE (dashed lines). For the original tag, the dielectric loading of PTFE shifts the resonance f_1 to 855 MHz, with the AT-code transition occurring at 838 MHz (Table V). Consequently, the AT code remains constant across the UHF band, as the resonance falls below the reader's operational range.

To shift this transition into the UHF band, specifically from 838 MHz to approximately 915 MHz, a positive frequency shift of 60–75 MHz is required. According to the characterization in Table VI, shortening the dipole arms by 4.2 cm provides the necessary offset. The solid lines in Fig. 14 illustrate the response of this 4.2 cm trimmed tag. The POTR resonance now aligns with the UHF band when placed on PTFE, resulting in a distinct, measurable AT-code transition. This confirms the tag has been successfully tuned for PTFE, enabling reliable material discrimination with a narrowband reader.

Note that, while this example optimizes the dipole length to shift the positive resonance marker f_1 into the UHF band, the design can also be tailored to shift the negative transition marker, f_a, into the reader's window. Furthermore, a single tag can be strategically optimized to provide multi-material detection: for instance, showing a positive AT-code transition, f_1, for one material and a negative transition, f_a, for another, effectively expanding the sensing range of an individual array element. By applying this systematic tuning to multiple tags, an array can be constructed where each element is tailored to a specific ε_{eff} range, as detailed in the following section.

C. Design and evaluation of a multi-material OD array

To demonstrate the practical utility of the proposed narrowband sensing approach, we designed a three-element OD tag array capable of discriminating between air and four distinct materials. The array consists of three Beontag A701 OD tags, individually optimized for a specific material by adjusting their dipole lengths to bring either the f_1 or f_a marker into the UHF band, as shown in Table VII.

TABLE VII
TARGET MATERIALS FOR EACH TAG IN THE ARRAY, TUNING LENGTH, AND SPECIFIC TRANSITION MARKERS FOR IDENTIFICATION

Array tag	**Trim length**	**Target MUT**	**In-band resonance**	**AT-code transition**
Tag 1 (top)	9 cm	PVC	f_1	Positive
		Rubber	f_a	Negative
Tag 2 (middle)	4.2 cm	PTFE	f_1	Positive
Tag 3 (bottom)	6.5 cm	Glass	f_a	Negative

Fig. 15(a) and (b) show the tag arrangement, with an inter-tag spacing of $d = 4.5$ cm, chosen so that the spacing between the tags (each of which has height 16 mm, see Table III) and spacing from the tag edges to the edges of Voyantic reference material sheet (130x130 mm) are all about the same, i.e., 10-12 mm. This strategic design allows the array to cover a

This article has been accepted for publication in IEEE Journal of Radio Frequency Identification. This is the author's version which has not been fully edited and content may change prior to final publication. Citation information: DOI 10.1109/JRFID.2026.3680834

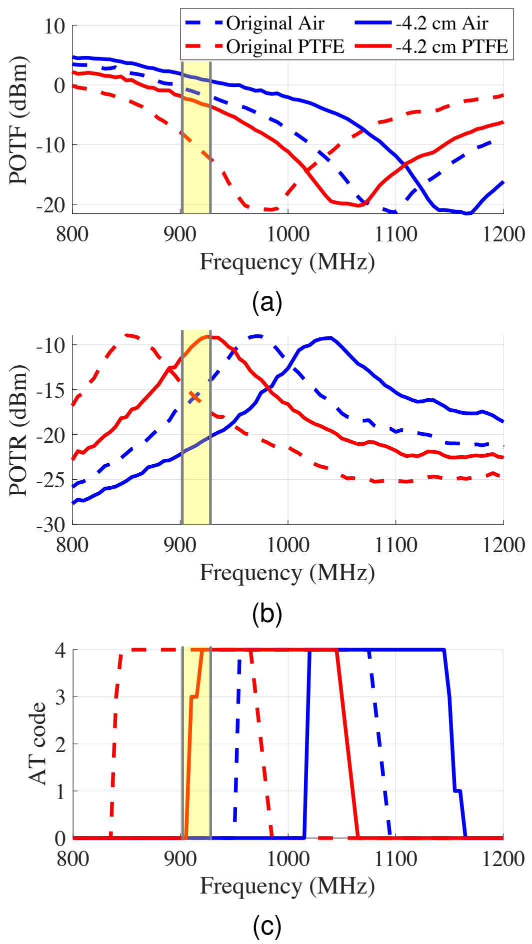

(a)

(b)

(c)

Fig. 14. (a) POTF, (b) POTR and (c) AT-code responses of a Beontag A701 OD tag in air, and on PTFE. Dashed lines correspond to the unmodified tag and solid lines to the tag trimmed 4.2 cm. The positive AT-code transition on PTFE for the trimmed tag falls within the UHF RFID band (in yellow).

broad range of permittivities while maintaining distinct, non-overlapping AT-code signatures for each material and no in-band resonances in the baseline air condition, as presented in the graph in Fig. 15(c).

Fig. 16 displays the measured AT-code responses obtained by sequentially interrogating each tag's EPC when placing the designed array on the four MUTs in Table VII. The AT-code transitions occur within the UHF band only when the array is in contact with the corresponding target material. When the array is on PVC, only a positive transition from Tag 1 is read in the UHF band, whereas when the array is on Rubber, only a negative transition from Tag 1 is visible. Similarly, when the array is on PTFE, only a positive transition from Tag 2 is read. Finally, for the glass sample, a negative transition is observed from Tag 3. Additionally, a negative transition from Tag 1 partially enters the UHF band. However, this does not compromise material differentiation, as the identification is based on the combined AT code transitions of all three tags in the array, rather than the response of a single tag, so the combined signatures remain distinct for each material.

These results confirm that the implemented OD tag array generates material-dependent, reproducible AT-code signatures and enables robust material discrimination using standard

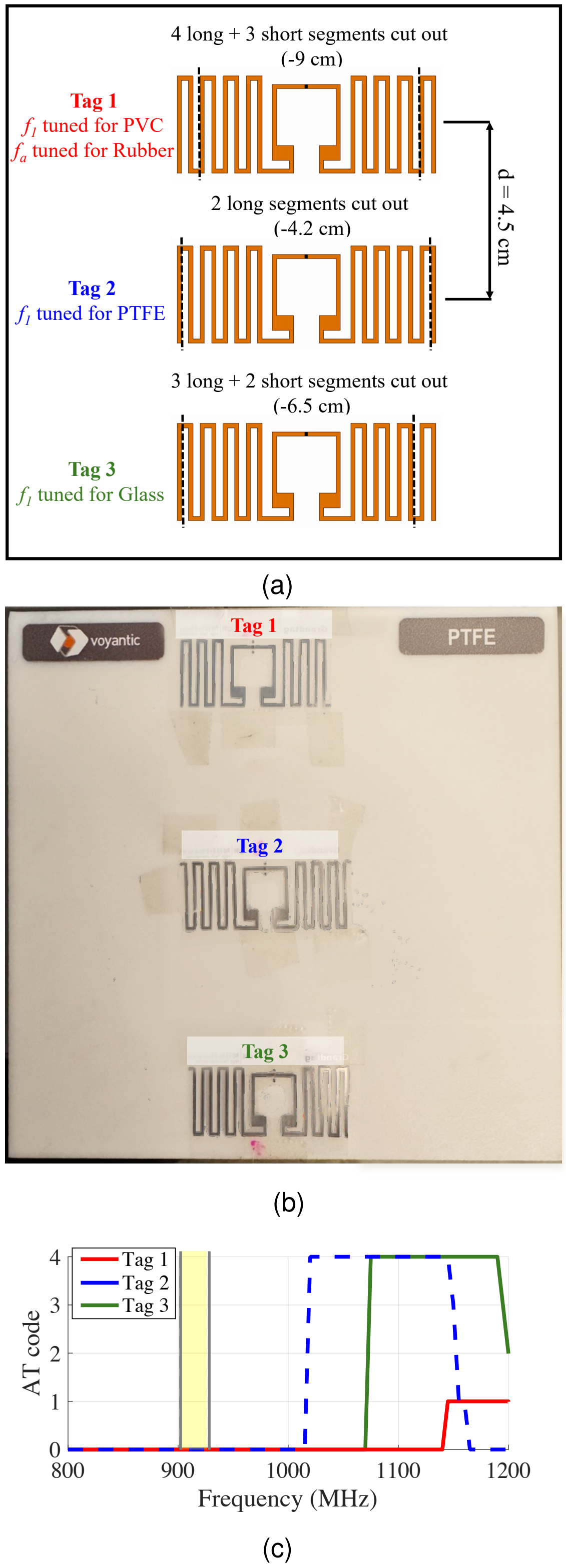

(a)

(b)

(c)

Fig. 15. (a) Designed OD tag array composed by three Beontag A701 OD tags tuned for four material detection and with an inter-tag spacing $d = 4.5$ cm, (b) photograph of the OD tag array on the PTFE sheet from Voyantic, and (c) individual AT-code responses of each tag in air with no in-band transition.

This article has been accepted for publication in IEEE Journal of Radio Frequency Identification. This is the author's version which has not been fully edited and content may change prior to final publication. Citation information: DOI 10.1109/JRFID.2026.3680834

narrowband readers by simply mapping the active transition in the UHF band to the specific tag's EPC.

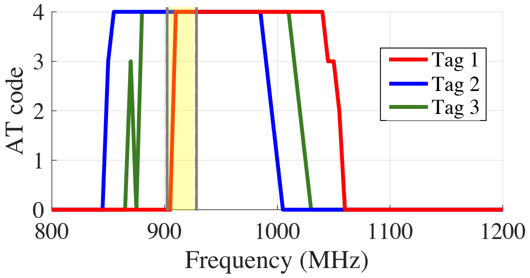

(a) OD Tag Array on PVC

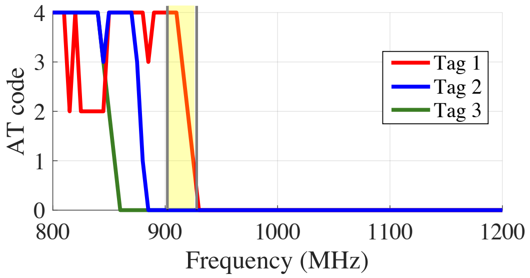

(b) OD Tag Array on Rubber

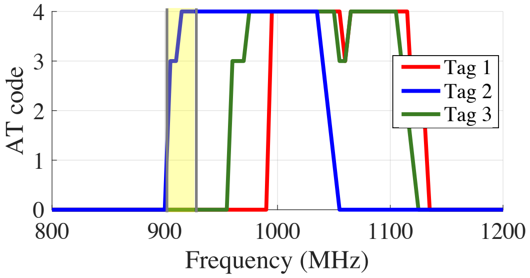

(c) OD Tag Array on PTFE

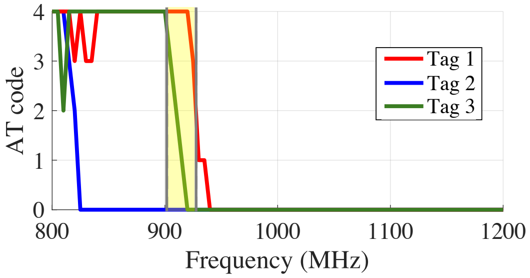

(d) OD Tag Array on Glass

Fig. 16. Measured AT-code responses of the implemented OD tag array attached to (a) PVC, (b) Rubber, (c) PTFE and (d) Glass. Since each tag is pre-tuned to a specific MUT, material identification is achieved by detecting which tag (i.e., EPC) undergoes a transition within the UHF RFID band (in yellow).

VII. CONCLUSIONS AND FUTURE WORK

In this paper, we investigated and experimentally demonstrated that RAIN RFID tags and arrays based on open dipole (OD) antennas offer a simplified, accurate, and practical solution for material sensing within the regularized UHF RFID band. By leveraging the inherent properties of the OD structure, we showed that these tags exhibit narrowband resonances free from the coupled modes and frequency-dependent distortions often found in traditional T-matched structures. This results in clear, predictable resonance markers (f_a and f_1) that provide enhanced flexibility for fine-tuning.

First, we showed how the effective permittivity, ε_{eff} of seven dielectric materials can be directly estimated from shifts in the f_a and f_c resonance frequencies extracted in three different ways. We evaluated these progressively more practical methods using six different RAIN RFID tags with distinct OD antenna designs and chips. In all cases, the estimated ε_{eff} values are consistent with those in the literature, with lower variance than those obtained using T-matched antennas on high ε_r dielectrics.

Secondly, our implementation of a three-element tag array demonstrated that by systematically trimming dipole lengths, distinct material signatures in the AT code changes across the UHF band can be mapped to specific tag IDs. We further showed that a single tag can provide bimodal sensing using a positive f_1 transition for one material and a negative f_a transition for another, thus increasing the information density of the array. These properties highlight the practical advantages of OD tags for robust, real-time material identification for standard, narrowband RFID infrastructure.

Future work will focus on extending and generalizing the proposed sensing framework in several directions. First, we plan to validate the robustness of AT-code–based resonance detection method under more realistic deployment conditions, such as using a commercial narrowband RFID reader with a fixed output power, measurements on real packaging materials with varying shapes and thicknesses, as well as dynamic scenarios where tagged items move through a conveyor-belt system. We also aim at exploring the use of the proposed methods for estimating the effective dielectric and magnetic properties of magneto-dielectric materials, such as flexible absorptive magnetic (FAM) sheets [15]. Further experimental studies will consider materials with higher relative permittivity and loss tangent, in order to assess the impact of material losses on features like POTF/POTR resonance magnitude and damping or AT-code transition slopes. In addition, we also aim to investigate the applicability of the presented techniques to other antenna geometries, with the goal of identifying resonance-based sensing principles beyond T-matched and open dipoles. With respect to the array-based approach, future efforts will examine the achievable dielectric and magnetic property sensing resolution as a function of tag tuning and array size, including exploring tag-to-tag coupling effects through simulations. Understanding these effects will allow us to design more scalable tag arrays that are not limited by spatial constraints such as material dimensions, for example through 3D arrangements of planar 2D tags or 3D tag structures [42]. Last but not least, we also plan to examine distinct machine learning approaches that will help automate material sensing.

This article has been accepted for publication in IEEE Journal of Radio Frequency Identification. This is the author's version which has not been fully edited and content may change prior to final publication. Citation information: DOI 10.1109/JRFID.2026.3680834

APPENDIX

A. Effect of the modulation resistance on POTR

Fig. 17 shows the narrowband circuit model of an RFID tag with an open dipole antenna introduced in [16], where the IC is modulated by $R_{mod} \ll R_p$, for most RFID chips.

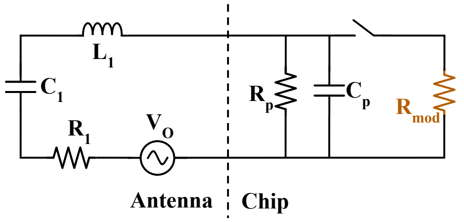

Fig. 17. Equivalent circuit of an RFID tag with an open dipole antenna [16]. R_{mod} is highlighted.

When $R_{mod} \to 0$, the IC's components C_p and R_p are shorted out, leaving C_1 as the only capacitive element in the LC-tank. This results in f_c (the POTR maximum) aligning with f_1. On the contrary, when $R_{mod} \gg 0$, the total capacitance becomes a series combination of C_1 and C_p. In this state, f_c shifts to align with f_a (the POTF minimum). Intermediate values of R_{mod} result in f_c falling between f_1 and f_a.

To illustrate the frequency-domain sensitivity of the POTR peak to R_{mod} variations, Fig. 18 presents the POTF/POTR curves for the A701 OD tag with an M700 IC. As R_{mod} increases, C_p starts affecting the POTR response, causing an upward shift in the resonant peak (f_c moves towards f_a) and a reduction in the quality factor (Q). As long as $R_{mod} \ll R_p$, the POTR resonance frequency, f_c, remains the same as the dipole resonance frequency, f_1 (which is POTR resonance frequency when $R_{mod} \to 0$). The POTF remains stationary, since it depends only on the antenna impedance and chip sensitivity, both of which are independent of the backscatter modulator.

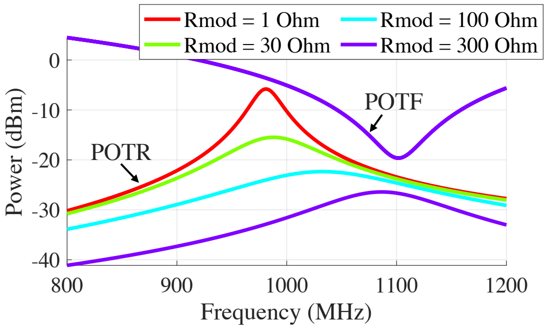

Fig. 18. POTF and POTR plots for A701 OD tag with M700 for different hypothetical R_{mod}. As R_{mod} increases, it affects POTR resonance while POTF remains the same.

B. Power Product equivalence

We consider a monostatic RFID reader with an ideal circulator (0 dB losses). Let G_r denote the reader antenna gain, and let L_path denote the one-way propagation path loss between reader and tag.

The power incident on the tag antenna is

$$P_\mathrm{inc} = P_\mathrm{TX}\, G_\mathrm{r}\, L_\mathrm{path}. \tag{12}$$

By definition, the threshold POTF is the incident power required to activate the RFID chip, i.e.,

$$\mathrm{POTF} = P_\mathrm{inc}. \tag{13}$$

The power backscattered by the tag at the antenna terminals is denoted as POTR, and the power received at the reader is therefore

$$P_\mathrm{RX} = \mathrm{POTR}\, G_\mathrm{r}\, L_\mathrm{path}. \tag{14}$$

Multiplying (12) and (14) yields

$$P_\mathrm{TX} \cdot P_\mathrm{RX} = \mathrm{POTF} \cdot \mathrm{POTR}. \tag{15}$$

Equation (15) shows that the product of transmitted and received reader powers at tag threshold is equal to the product of POTF and POTR.

C. Independence of Power Product on the propagation path

The power absorbed by the RFID chip at threshold (i.e., IC sensitivity) can be written as

$$P_\mathrm{ic} = \mathrm{POTF}\, p\, G_\mathrm{tag}\, \tau, \tag{16}$$

where G_tag is the tag antenna gain, p is the polarization mismatch factor between reader and tag antennas, and τ is the impedance matching coefficient between antenna impedance Z_a and chip impedance Z_c, given by

$$\tau = \frac{4R_cR_a}{|Z_c + Z_a|^2}. \tag{17}$$

The backscattered power can be expressed as [12]

$$\mathrm{POTR} = \mathrm{POTF}\, K, \tag{18}$$

where K is the backscatter coefficient

$$K = Mp^2G_\mathrm{tag}^2 = \frac{1}{4}|\Delta\Gamma|^2p^2G_\mathrm{tag}^2. \tag{19}$$

Here, $M = \frac{1}{4}|\Delta\Gamma|^2$ is the modulation factor, where the constant 1/4 depends on the reader Received Signal Strength Indicator (RSSI) definition and is typical for most RFID readers [43]. $\Delta\Gamma$ is the difference between the complex reflection coefficients, ρ corresponding to the chip's two modulation states,

$$\Delta\Gamma = \rho_c - \rho_m, \tag{20}$$

with

$$\rho_c = \frac{Z_c - Z_a^*}{Z_c + Z_a}, \qquad \rho_m = \frac{Z_m - Z_a^*}{Z_m + Z_a}. \tag{21}$$

Under the common assumption that the modulating impedance satisfies $Z_m \to 0$ [12],

$$\rho_m \approx -\frac{Z_a^*}{Z_a}. \tag{22}$$

Substituting into $\Delta\Gamma$ yields

$$\Delta\Gamma = \frac{2R_aZ_c}{Z_a(Z_c + Z_a)}. \tag{23}$$

This article has been accepted for publication in IEEE Journal of Radio Frequency Identification. This is the author's version which has not been fully edited and content may change prior to final publication. Citation information: DOI 10.1109/JRFID.2026.3680834

Using (16)–(23), the power-product expression becomes

$$\mathrm{POTF} \cdot \mathrm{POTR} = \frac{P_{\mathrm{ic}}^2}{4} \frac{|\Delta\Gamma|^2}{\tilde{\tau}^2}, \tag{24}$$

or equivalently,

$$\mathrm{POTF} \cdot \mathrm{POTR} = P_{\mathrm{ic}}^2 \cdot \frac{|Z_c + Z_a|^2}{16 R_c^2} \cdot \frac{|Z_c|^2}{|Z_a|^2}, \tag{25}$$

which depends only on the antenna and chip impedances and IC sensitivity, and is independent of the propagation path and tag antenna gain.

D. Conjugate matching of the antenna reactance

Fig. 19 shows two analogous representations of an RFID tag with an auto-tuning (AT) IC. In the top circuit, the antenna impedance is represented as a series impedance, $Z_a = R_a + jX_a$, whereas the in the bottom one, it is represented as a parallel impedance, $1/Z_a = 1/R_{pa} + 1/jX_{pa}$. The latter allows to better observe the complex conjugate matching condition between the antenna and the IC: to achieve impedance matching, the chip's effective parallel capacitance, C_{needed}, needs to be adjusted to conjugately match the antenna parallel reactance, X_{pa}.

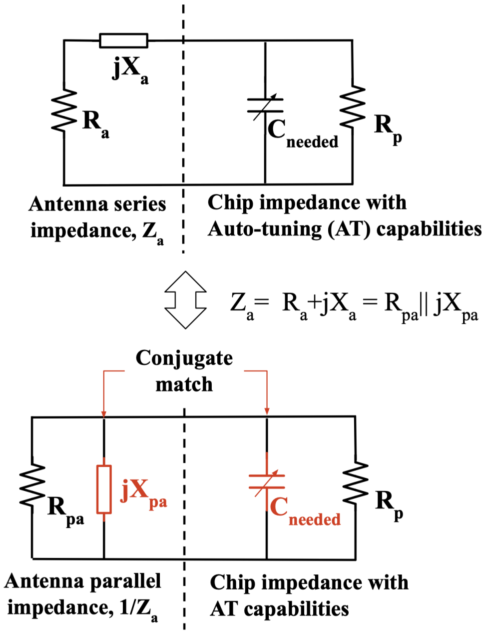

Fig. 19. Equivalent circuits of an RFID tag with AT capabilities with series antenna impedance, Z_a (top) and parallel antenna impedance $1/Z_a$ (bottom).

From the top circuit,

$$\frac{1}{Z_a} = \frac{1}{R_a + jX_a} = \frac{R_a}{R_a^2 + X_a^2} - \frac{jX_a}{R_a^2 + X_a^2}, \tag{26}$$

and from the bottom circuit,

$$\frac{1}{Z_a} = \frac{1}{R_{pa}} + \frac{1}{jX_{pa}} = \frac{1}{R_{pa}} - \frac{j}{X_{pa}}. \tag{27}$$

From (26) and (27), it can be deduced that X_{pa} depends on both the series resistance and reactance of the antenna, such that

$$jX_{pa} = j\frac{R_a^2 + X_a^2}{X_a}. \tag{28}$$

Finally, to achieve impedance matching,

$$\frac{1}{j\omega C_{\mathrm{needed}}} = -jX_{pa}, \tag{29}$$

which leads to (9) in the paper:

$$C_{\mathrm{needed}} = \frac{1}{\omega X_{pa}} = \frac{X_a}{\omega\left(R_a^2 + X_a^2\right)}. \tag{30}$$

REFERENCES

[1] Impinj, "From TikTok to Tariffs: Impinj Supply Chain Integrity Outlook 2026 Reveals Growing Strain Between Consumer Expectations and Supply Chain Reality." [Online]. Available: https://tinyurl.com/impinj-2026.

[2] Think WIoT, "Structural Health Monitoring with Sensor-Based RFID Tags." [Online]. Available: https://wiot-group.com/think/en/articles/structural-health-monitoring-with-sensor-based-rfid-tags/, 2024.

[3] H. Z. et al., "NFC/RFID-enabled wearables and implants for biomedical applications," *Microsyst Nanoeng*, vol. 11, no. 191, 2025.

[4] T. Taylor, "From Hardware to Software: How RFID Is Transforming Retail." [Online]. Available: https://www.abiresearch.com/blog/rfid-in-retail.

[5] N. Eaton, "Walmart expands RFID mandate: What it means for RAIN RFID in retail." [Online]. Available: www.impinj.com/library/blog/walmart-makes-big-rfid-commitment-with-sweeping-tag-mandate.

[6] S.A.R. Khan et al., "A recent digitalization in recycling industry attaining ecological sustainability: A comprehensive outlook and future trend," *Environ Sci Pollut Res*, no. 30, p. 103760–103775, 2023.

[7] J.P. Harrison et al., "Biodegradability standards for carrier bags and plastic films in aquatic environments: A critical review," *R. Soc. open sci*, vol. 5, p. 171792, 2018.

[8] Villa-Gonzalez, F. et al., "Single and bulk identification of plastics in the recycling chain using chipless RFID tags," in *2021 IEEE RFID*, pp. 1–8, 2021.

[9] Voyantic TagFormance Pro. [Online]. Available: https://voyantic.com/lab/tagformance-pro/.

[10] Mohammed, N. A. et al., "Analysis and synthesis of UHF RFID antennas using the embedded T-match," in *2010 IEEE International Conference on RFID (IEEE RFID 2010)*, pp. 230–236, 2010.

[11] ARC program. [Online]. Available: https://rfid.auburn.edu/arc.

[12] Nikitin, P. et al., "RFID tag analysis using an equivalent circuit," in *2021 IEEE Int. Symp. APS/URSI*, pp. 167–168, 2021.

[13] P. Nikitin et al., "Dielectric sensing using T-matched RAIN RFID tags," in *IEEE RFID*, pp. 42–47, 2023.

[14] R. Bhattacharyya et al., "Representation Learning Using RAIN RFID Tag Backscatter Features for Material Classification in Circular Economy Applications," in *IEEE RFID*, pp. 1–6, 2025.

[15] P. Nikitin et al., "Magnetic sensing using T-matched RAIN RFID tags," in *2024 IEEE RFID*, pp. 1–6, 2024.

[16] P. Nikitin et al., "Equivalent Circuit Analysis of RFID Tags with Open Dipole Antennas," in *2025 IEEE AP-S/CNC-USNC-URSI*, pp. 2610–2613, 2025.

[17] P. Basset et al., "Chip-size antennas for implantable sensors and smart dust," in *The 13th International Conference on Solid-State Sensors, Actuators and Microsystems, 2005. Digest of Technical Papers. TRANSDUCERS '05.*, vol. 1, pp. 457–460 Vol. 1, 2005.

[18] Y. Yamada, W. H. Jung, and N. Michishita, "Extremely Small Antennas for RFID Tags," in *2006 10th IEEE Singapore International Conference on Communication Systems*, pp. 1–5, 2006.

[19] J. Grosinger et al., "Passive RFID Sensor Tag Concept and Prototype Exploiting a Full Control of Amplitude and Phase of the Tag Signal," *IEEE Trans. Microw. Theory Techn.*, vol. 64, no. 12, pp. 4752–4762, 2016.

[20] D. M. Dobkin and S. M. Weigand, "Environmental Effects on RFID Tag Antennas," in *IEEE MTT-S IMS Digest*, (Long Beach, CA, USA), pp. 135–138, 2005.

[21] P. Nikitin, K. V. S. Rao, and S. Lam, "UHF RFID Tag Characterization: Overview and State-of-the-Art," in *Antenna Measurement Techniques Association (AMTA) conference*, (Seattle, WA), 2012.

[22] P. Nikitin, J. Kim, and K. V. S. Rao, "Analysis of UHF RFID Tag Antennas Using an Equivalent Circuit Approach," *IEEE J. RFID*, vol. 10, pp. 136–149, 2026.

[23] G. Marrocco, "RFID Grids: Part I—Electromagnetic Theory," *IEEE Trans. Antennas Propag.*, vol. 59, no. 3, pp. 1019–1026, 2011.

[24] C. Occhiuzzi and G. Marrocco, "Precision and Accuracy in UHF-RFID Power Measurements for Passive Sensing," *IEEE Sens. J.*, vol. 16, no. 9, pp. 3091–3098, 2016.

[25] M. C. Caccami and G. Marrocco, "Electromagnetic Modeling of Self-Tuning RFID Sensor Antennas in Linear and Nonlinear Regimes," *IEEE Trans. Antennas Propag.*, vol. 66, no. 6, pp. 2779–2787, 2018.

[26] S. Caizzone and G. Marrocco, "RFID Grids: Part II—Experimentations," *IEEE Trans. Antennas Propag*, vol. 59, no. 8, pp. 2896–2904, 2011.

[27] C. Li et al., "Radio frequency identification sensing techniques and systems for structural health monitoring - a review of the state-of-the-art," *IEEE Internet of Things Journal*, pp. 1–1, 2026.

[28] C. Occhiuzzi et al., "RFID epidermal sensor including hydrogel membranes for wound monitoring and healing," in *2015 IEEE International Conference on RFID (RFID)*, pp. 182–188, 2015.

[29] C. Occhiuzzi, S. Caizzone, and G. Marrocco, "Passive UHF RFID Antennas for Sensing Applications: Principles, Methods, and Classifications," *IEEE Antennas Propag. Mag.*, vol. 55, no. 6, pp. 14–34, 2013.

[30] Mark Cotton, Impinj, "Read AutoTune value in Voyantic Tagformance threshold measurements." [Online]. Available: https://support.impinj.com/hc/en-us/articles/360016583919-Read-AutoTune-Value-in-Voyantic-Tagformance-Threshold-Measurements.

[31] R. Bhattacharyya et al., "Material Sensing Using RAIN RFID Tags With Auto-Tuning Capabilities," *IEEE J. RFID*, vol. 9, pp. 340–349, 2025.

[32] F. Naccarata, G. M. Bianco, and G. Marrocco, "Sensing performance of multi-channel RFID-based finger augmentation devices for Tactile Internet," *IEEE J. RFID*, vol. 6, pp. 209–217, 2022.

[33] Dutta, D. et al., "Characterization of material resistivity by using a self-tunable chip for gas sensing application," in *2024 IEEE AP-S/INC-USNC-URSI*, pp. 1611–1612, 2024.

[34] N. Barbot et al., "Simple low cost open source UHF RFID reader," *IEEE Journal of Radio Frequency Identification*, vol. 7, pp. 20–26, 2023.

[35] Beontag A701. [Online]. Available: https://tinyurl.com/atlasrfidstore.

[36] Mike Lenehan, Impinj, "Impinj M700 Series Tag Chips Product Brief." [Online]. Available: https://support.impinj.com/article/360010797539. Accessed on: March. 23, 2026.

[37] Mike Lenehan, "AutoTune Technology White Paper," tech. rep., Impinj, 2019.

[38] AXZON, "Axzon Application Note AN002F40: Reading Magnus-S Sensors," tech. rep., 2025.

[39] Impinj, "RAIN RFID Tags from Impinj Partners." [Online]. Available: https://www.impinj.com/partners/products/partner-tags?pagesize=500.

[40] Voyantic, "Reference Material Set." [Online]. Available: https://voyantic.com/lab/tagformance-pro/accessories/.

[41] A. Abbosh, "Accurate Effective Permittivity Calculation of Printed Center-Fed Dipoles and Its Application to Quasi Yagi-Uda Antennas," *IEEE Trans. Antennas Propag.*, vol. 61, pp. 2297–2300, apr 2013.

[42] M. Hasani, L. Sydänheimo, and L. Ukkonen, "Design and implementation of fully 3D miniaturized passive UHF RFID tag for sensing applications," in *2015 LAPC*, pp. 1–4, 2015.

[43] J. D. Griffin and G. D. Durgin, "Complete Link Budgets for Backscatter-Radio and RFID Systems," *IEEE Antennas Propag. Mag.*, vol. 51, no. 2, pp. 11–25, 2009.

Fatima Villa-Gonzalez (Member, IEEE) received the Ph.D. degree in Electrical and Electronics Engineering from Tecnun, University of Navarra, Spain, in 2023. She completed her Bachelor in Telecommunications Systems Engineering and M.Sc. degree in Telecommunications Engineering from Tecnun in 2017 and 2019, respectively. She joined MIT Auto-ID Labs in 2019 and has been closely working with them since then, where she is currently a Postdoc Associate. She is interested in applied research related to wireless sensors, chipped and chipless RFID sensors, antennas and signal processing. She was the recipient of the 2024 IEEE RFID-TA Conference Women Best Paper Award.

Rahul Bhattacharyya (Senior Member, IEEE) received the Ph.D. degree in Systems Engineering from the Massachusetts Institute of Technology, Cambridge, MA, USA, in 2012. He is currently the Director of the Auto-ID Labs at MIT, where his research encompasses the development and integration of technologies that form the framework for the Internet of Things. He is an Associate Editor for the IEEE Sensors Journal. He has also served as the TPC Chair of IEEE RFID 2018-19 and the 4th International Conference on the Internet of Things (IoT 2014) at MIT. He has authored over 50 technical peer reviewed publications. He was the recipient of the 2020 IEEE Sensors and 2015 IEEE RFID-TA Conference Best Paper Award. He has also been awarded 2 US and 2 international patents for his work.

Pavel Nikitin (Fellow, IEEE) received the Ph.D. degree in electrical and computer engineering from Carnegie Mellon University in 2002. He is currently a Technical Fellow with Impinj, Inc., Seattle, WA, USA, where he is doing research, design, and development of RAIN RFID tags and systems products. Previously, he worked at Honeywell, Intermec, IBM, and Ansys. He is also an Affiliate Associate Professor with the Electrical and Computer Engineering Department, University of Washington. He received four best paper awards, has over 70 IEEE publications, and over 80 U.S. and international patents.